Global and Planetary Change 123 (2014) 110–120

Contents lists available at ScienceDirect

Global and Planetary Change

journal homepage: www.elsevier.com/locate/gloplacha

Isotopic evidence for water-column denitrification and sulfate reduction at the end-Guadalupian (Middle Permian)

Masafumi Saitoh [a,b,*], Yuichiro Ueno [a,c], Yukio Isozaki [d], Manabu Nishizawa [b], Katsumi Shozugawa [e], Tetsuya Kawamura [a], Jianxin Yao [f], Zhansheng Ji [f], Ken Takai [b,c,g], Naohiro Yoshida [c,h], Motoyuki Matsuo [e]

[a] Department of Earth and Planetary Sciences, Tokyo Institute of Technology, Meguro, Tokyo 152-8551, Japan
[b] Laboratory of Ocean-Earth Life Evolution Research (OELE), Japan Agency for Marine-Earth Science and Technology (JAMSTEC), Natsushima-cho, Yokosuka 237-0061, Japan
[c] Earth-Life Science Institute, Tokyo Institute of Technology, Meguro, Tokyo 152-8551, Japan
[d] Department of Earth Science and Astronomy, The University of Tokyo, Meguro, Tokyo 153-8902, Japan
[e] Department of Chemistry, The University of Tokyo, Meguro, Tokyo 153-8902, Japan
[f] Geology Institute, Chinese Academy of Geological Science, Beijing 100037, China
[g] Department of Subsurface Geobiological Analysis and Research (D-SUGAR), Japan Agency for Marine-Earth Science and Technology (JAMSTEC), Natsushima-cho, Yokosuka 237-0061, Japan
[h] Department of Environmental Chemistry and Engineering, Tokyo Institute of Technology, Midori, Yokohama 226-8503, Japan

ARTICLE INFO

Article history:
Received 23 October 2013
Received in revised form 16 October 2014
Accepted 24 October 2014
Available online 5 November 2014

Keywords:
Capitanian
disphotic zone
denitrification
sulfate reduction
sulfidic deep-water
extinction

ABSTRACT

The total nitrogen and pyrite sulfur isotopic compositions of the Guadalupian–Lopingian (Middle-Upper Permian) shelf carbonates are analyzed at Chaotian in northern Sichuan, South China, to clarify the environmental changes in the relatively deep disphotic zone (generally deeper than 150 m) in the ocean at the end-Guadalupian, focusing on the possible relationships with the deep-sea oxygen depletion and the shallow-sea extinction. At Chaotian, the Guadalupian Maokou Formation and the Early Lopingian Wujiaping Formation are primarily composed of bioclastic limestone of shallow-water facies, although the topmost part of the Maokou Formation (ca. 11 m thick) is composed of bedded black mudstone and chert that was deposited on the disphotic slope/basin under anoxic conditions. Substantially high $\delta^{15}N$ values of total nitrogen (up to +14‰) in the topmost Maokou Formation of the deep-water facies indicate water-mass denitrification. In the same disphotic interval, the consistently low $\delta^{34}S$ values of pyrite (ca. −37‰) suggest sulfate reduction in the sulfate-rich water column. The new nitrogen and sulfur isotopic records at Chaotian indicate the enhanced anaerobic respiration in the oxygen-depleted disphotic zone in the Late Guadalupian in northwestern South China. The active water-column sulfate reduction likely resulted in the emergence of a sulfidic deep-water mass on the disphotic slope/basin, which is supported by the high proportions of pyrite Fe to highly reactive Fe in the rocks shown using ^{57}Fe Mössbauer spectroscopy. The anaerobic respiration in the disphotic zone at the end-Guadalupian may have been enhanced by an expansion of the oxygen minimum zone (OMZ) caused by the increased primary productivity in the surface oceans; the OMZ expansion may have corresponded to the onset of prolonged oxygen depletion in the deep sea. The clear stratigraphic relationship at Chaotian shows the emergence of the sulfidic deep-waters preceding the extinction, implying that the upwelling of the sulfidic deep-water from the previously overlooked disphotic zone to the shallow shelves along the continental margin may have acted as a stress to the shallow-marine biota.

1. Introduction

The end-Guadalupian (Middle Permian) extinction event (ca. 260 Ma) is one of largest biodiversity crises in the Phanerozoic and preceded the latest Permian extinction by ca. 800 million years (Jin et al., 1994; Stanley and Yang, 1994; Gradstein et al., 2012). Near the Guadalupian–Lopingian (Late Permian) boundary (G–LB), various geologic phenomena in addition to the extinction have been emphasized, including: (1) the eruption of the Emeishan flood basalts in South China (Chung and Jahn, 1995; Zhou et al., 2002); (2) the onset of prolonged oxygen depletion in the deep sea (superanoxia; Isozaki, 1997); (3) one of the lowest sea levels in the Phanerozoic (Jin et al., 1994; Haq and Schutter, 2008); (4) one of the lowest $^{87}Sr/^{86}Sr$ ratios in the Phanerozoic (Veizer et al., 1999; Kani et al., 2008); (5) a highly positive plateau interval of the stable carbon isotope (up to +5‰) named the 'Kamura event' (Isozaki et al., 2007); and (6) the onset of frequent geomagnetic polarity changes (Illawarra Reversal; Irving and Parry, 1963; Isozaki, 2009b). These events may have been related to the biotic crisis observed on the continental shelves at the end-Guadalupian (Isozaki, 2009a). In particular, the eruption of the Emeishan flood basalts has been the leading candidate for the ultimate

* Corresponding author at: 2-15 Natsushima-cho, Yokosuka 237-0061, Japan. Tel.: +81 46 867 9658.
E-mail address: saitoh.m.ab@jamstec.go.jp (M. Saitoh).

http://dx.doi.org/10.1016/j.gloplacha.2014.10.014
0921-8181/

cause of the shelf extinction because of its temporal correspondence with the extinction (e.g., Wignall et al., 2009); however, the causal link between the environmental changes around the G–LB and the extinction remains a topic of discussion (e.g., Clapham et al., 2009; Bond et al., 2010; Jost et al., 2014).

Previous stratigraphic studies across the G–LB have primarily focused on fossiliferous shallow-marine shelf carbonates and deep-sea cherts (e.g., Jin et al., 1994; Isozaki, 1997; Kato et al., 2002). The shallow-marine fossil records in the shelf carbonates have demonstrated the severe extinction in the shallow sea, whereas petrological and geochemical analyses of the deep-sea cherts have suggested the onset of a prolonged oxygen depletion in the deep sea at the end-Guadalupian. However, additional information from the relatively deep disphotic zone in the oceans (typically deeper than 150 m) is critical for the overall evaluation of the environmental changes in the oceans and, particularly, for understanding the relationships between the shallow-sea extinction and the deep-sea oxygen depletion. To examine the environmental changes in the previously overlooked disphotic zone in the ocean around the G–LB, we have analyzed the Guadalupian–Lopingian shelf carbonates of the deep-water facies at the Chaotian section in northern Sichuan, South China (Fig. 1a,b; Isozaki et al., 2004, 2008; Saitoh et al., 2013a,b). Isozaki et al. (2008) and Saitoh et al. (2013a) clarified the emergence of oxygen-depleted conditions on the disphotic slope/basin prior to the end-Guadalupian extinction at Chaotian based on the characteristics of the litho- and bio-facies.

Generally, nitrate and sulfate are thought to be important oxidants in the oceanic biogeochemical cycles, particularly under oxygen-depleted conditions (e.g., Jørgensen, 1982; Codispoti and Christensen, 1985). The isotopic compositions of nitrogen and sulfur compounds in sedimentary rocks are useful to understand the nitrogen and sulfur cycles, respectively, in past oceans (e.g., Canfield, 2001a; Robinson et al., 2012). In this study, we report the total nitrogen and pyrite sulfur isotope chemostratigraphy of the Guadalupian–Lopingian carbonates at Chaotian to investigate the fluctuations in the nitrogen and sulfur cycles in the oxygen-depleted disphotic zone around the G–LB. We also analyzed the chemical states of the iron in the rocks by ^{57}Fe Mössbauer spectroscopy to examine the redox conditions on the disphotic slope/basin in northwestern South China in more detail. Based on the new geochemical results at Chaotian, we discuss the environmental changes in the disphotic zone in the ocean at the end-Guadalupian and their possible link to the shallow-sea extinction and the deep-sea oxygen depletion.

2. Geological setting and stratigraphy

During the Permian, South China was located on the eastern side of Pangea around the equator, and shallow-marine carbonates and terrigenous clastics with diverse fossils were extensively deposited on its continental shelves (Fig. 1b; Zhao et al., 1981; Scotese and Langford, 1995; Jin et al., 1998). Shelf-carbonates of relatively deep-water facies thickly accumulated in a shelf/slope setting in northern Sichuan along the northwestern edge of South China (Fig. 1b; Wang and Jin, 2000). We have analyzed the Guadalupian–Lopingian carbonates deposited on the relatively deep shelf/slope at Chaotian in northern Sichuan (32°37′N, 105°51′E; Fig. 1; Isozaki et al., 2004, 2008; Saitoh et al., 2013a,b). The analyzed carbonate rocks (ca. 60 m thick) at Chaotian are composed of the following three stratigraphic units: (1) the early Capitanian (Late Guadalupian) Limestone Unit of the Maokou Formation; (2) the early–late Capitanian Mudstone Unit of the Maokou Formation; and (3) the lower part of the early Wuchiapingian (Early Lopingian) Wujiaping Formation, in ascending order (Fig. 1c; Isozaki et al., 2008; Lai et al., 2008; Saitoh et al., 2013a). The Limestone Unit of the Maokou Formation is composed of massive bioclastic limestone with abundant shallow-marine fossils (e.g., calcareous algae, fusulines, and corals) deposited on a euphotic shelf (generally shallower than 150 m) under oxic conditions.

In contrast, the Mudstone Unit is primarily composed of bedded black calcareous mudstone, black chert/siliceous mudstone, and dark gray muddy carbonates containing abundant radiolarians, conodonts, and ammonoids (Fig. 1c; Isozaki et al., 2008; Saitoh et al., 2013a). The characteristics of the litho- and bio-facies indicate that the Mudstone Unit was deposited on a relatively deep disphotic slope/basin, generally deeper than 150 m in the modern oceans, under anoxic conditions (Saitoh et al., 2013a). In contrast, the overlying lower Wujiaping Formation is composed of bioclastic limestone with shallow-marine fossils, such as calcareous algae; the sedimentary environment returned from the disphotic slope/basin to the euphotic shelf across the G–LB. This shallowing across the G–LB at Chaotian most likely recorded a global sea-level drop based on the stratigraphic correlations around the world (Saitoh et al., 2013a). Haq and Schutter (2008) roughly estimated that the sea-level fell at most 100 m on a global scale at the end-Guadalupian. Because the sedimentary environment returned to the euphotic shelf (generally shallower than 150 m) as a result of this sea-level decrease of less than 100 m, the Mudstone Unit at Chaotian was likely deposited at a depth shallower than 250 m. Considering these upper and lower limits of the water depth, it is estimated that the Mudstone Unit at Chaotian was deposited on the disphotic slope/basin in northwestern South China at a depth of between 150 and 250 m.

3. Analytical methods

Rock samples were collected from the outcrop by field research and from deeper than 150 m below the surface by scientific drilling. For all of the geochemical analyses, fresh rock samples were carefully chosen based on detailed observations of polished slabs and thin sections under the petrographic microscope. In particular, the exceptionally fresh drill core samples were analyzed in the Mudstone Unit of the Maokou Formation at Chaotian.

3.1. Nitrogen and organic carbon isotope analyses

Powdered sample (0.5–6.0 g) was treated with 10 M HCl for >24 h, and all of the carbonate was dissolved. After the reaction, the residue was separated by repeated centrifugation with the addition of distilled water; the sample was then dried at 70 °C for >12 h. The residue was then placed in a tin cup, and the total nitrogen and organic carbon isotopic values and the total nitrogen (TN) and total organic carbon (TOC) contents were measured using a ThermoFinnigan DELTAplus Advantage mass spectrometer coupled with an EA 1112 Series FLASH Elemental Analyzer at the Japan Agency for Marine-Earth Science and Technology (JAMSTEC). Saitoh et al. (2013a) preliminarily reported the TOC contents of the sedimentary rocks across the G–LB at Chaotian; we added new TOC data in the present study. The nitrogen and carbon isotopic compositions are reported in ‰ relative to atmospheric N_2 and to the Vienna Peedee Belemnite (V-PDB) standard, respectively, according to $\delta^{15}N = (R_{sample} / R_{standard} - 1) \times 1000$ and $\delta^{13}C_{org} = (R_{sample} / R_{standard} - 1) \times 1000$, respectively, where R is the isotopic ratio ($^{15}N/^{14}N$ and $^{13}C/^{12}C$, respectively) of the sample and the standard. The analytical reproducibility of the $\delta^{15}N$ and $\delta^{13}C_{org}$ values determined by replicate analyses of the laboratory standards is better than 0.3‰ and 0.2‰ (1σ), respectively.

3.2. Sulfur isotope analysis

Powdered sample (0.5–30.0 g) was ultrasonically washed and then soaked in a 10% NaCl solution for 24 h, rinsed with distilled water and centrifuged to remove the soluble sulfate. The residue was then washed and soaked in acetone for 24 h to dissolve the elemental sulfur, rinsed with distilled water and centrifuged. The residue was dried for >24 h at room temperature. The sulfide was extracted by a method modified

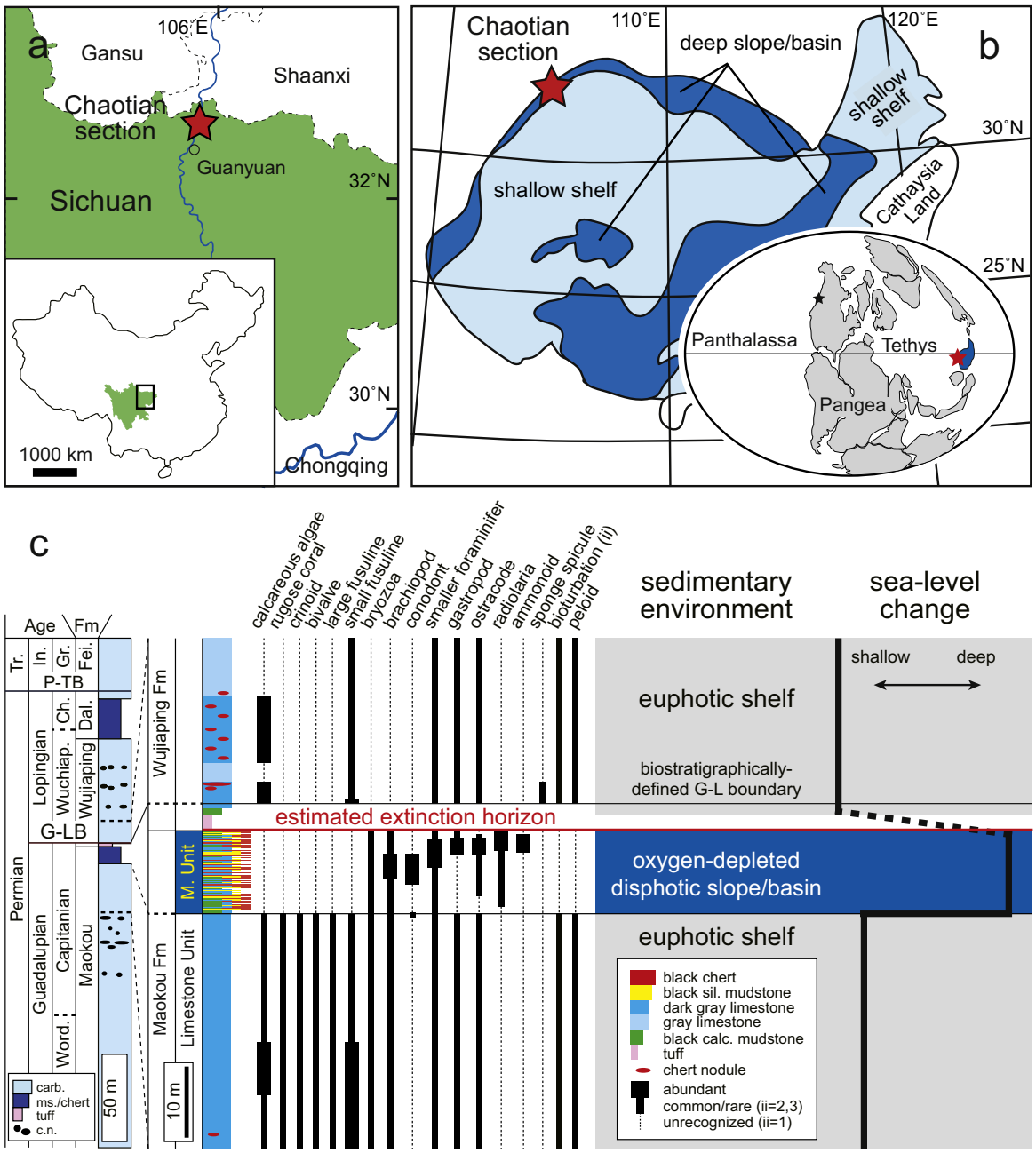

Fig. 1. Stratigraphy at Chaotian. (a) Location of the Chaotian section. (b) Paleogeography of South China in the Capitanian (Late Guadalupian) modified from Wang and Jin (2000). The global paleogeography is also shown in the inset. South China is shown in dark blue, and the red and black stars represent the locations of Chaotian and Opal Creek, respectively. (c) Stratigraphy across the Guadalupian–Lopingian (Middle-Upper Permian) boundary (G–LB) at Chaotian. The ranges of the fossil groups, the sea-level changes and the sedimentary environments are modified from Saitoh et al. (2013a). carb.: carbonate; ms.: mudstone; calc.: calcareous; sil.: siliceous; c.n.: chert nodule; ii: ichnofabric index; M.: Mudstone; Word.: Wordian; Wuchiap.: Wuchiapingian; Ch.: Changhsingian; Dal.: Dalong; Tr.: Triassic; In.: Induan; Gr.: Griesbachian; Fei.: Feixianguan; P–TB: Permian–Triassic boundary. (For interpretation of the references to color in this figure legend, the reader is referred to the web version of this article.)

from Hsieh and Shieh (1997). Less than 5 g of the dried residue and an alkaline Zn trap were placed into a 500 ml glass bottle with two stopcocks; the bottle was purged with nitrogen and then the sample was reacted with 20 ml of 5 M HCl and subsequently with a 20 ml chromium(II) solution for >48 h at room temperature (Canfield et al., 1986). Chromium(II)-reducible sulfur (CRS) was reduced to H_2S and then precipitated as ZnS in a 20 ml alkaline Zn trap. In this extraction procedure, acid volatile sulfur (AVS) is also reduced to H_2S and precipitated as ZnS, although our preliminary analysis showed that only a small amount of AVS is contained in the rock samples at Chaotian (data not shown). ZnS was then converted to Ag_2S by reaction with 0.1 M $AgNO_3$. The resulting Ag_2S was cleaned by repeated centrifugation using distilled water and dried at 70 °C for >12 h. The CRS contents of certain samples were low, and more than 5 g of the powdered sample was required to obtain a sufficient amount of Ag_2S for isotopic analysis. When an excessive amount of powdered sample is placed in a single glass bottle, it cannot react completely with HCl and the chromium(II) solution. In that case, we extracted CRS in several glass bottles and combined it after conversion to Ag_2S.

For the isotopic analyses, Ag_2S was reacted with excess F_2 at 300 °C in a nickel reaction tube overnight to produce SF_6, which was then purified using cryogenic techniques and gas chromatography. The isotopic composition of SF_6 was determined using a ThermoFinnigan MAT253 mass spectrometer equipped with a dual inlet system at the Tokyo Institute of Technology. The sulfur isotopic compositions are reported in ‰ relative to the Vienna Canion Diabro Troilite (V-CDT) standard

according to $\delta^{34}S = (R_{sample} / R_{standard} - 1) \times 1000$, where R is the isotopic ratio ($^{34}S/^{32}S$) of the sample and the standard. The analytical reproducibility of the $\delta^{34}S$ values determined by replicate analyses of the international reference material, IAEA-S1, is 0.4‰ (1σ).

3.3. ^{57}Fe Mössbauer spectroscopic analysis

To investigate the redox conditions of the Mudstone Unit at Chaotian in detail, we analyzed the chemical states of the iron in the rock samples by ^{57}Fe Mössbauer spectroscopy (Matsuo et al., 2003). In this method, gamma-ray absorption spectra of the iron in the analyzed sample are measured utilizing the resonance absorption of a gamma ray by an iron nucleus called the Mössbauer effect (e.g., Tominaga and Minai, 1984). The peak number and positions of the absorption spectrum reflect an interaction between the nucleus and the surrounding electrons, providing information on the chemical states of the iron in the sample. The ^{57}Fe Mössbauer spectroscopic analysis is a useful method for clarifying the chemical states of iron in geological samples, such as deep-sea pelagic chert (Sato et al., 2011), without a sequential wet extraction procedure.

For the present analysis, black calcareous mudstone and dark gray muddy limestone samples with relatively high iron contents in the Mudstone Unit at Chaotian were chosen. Powdered sample (ca. 400 mg) was mounted in a sample holder (16 mm in diameter, 2 mm thick); the Mössbauer spectra were measured with an Austin Science S-600 Mössbauer spectrometer at the University of Tokyo using a 1.11 GBq ^{57}Co/Rh source at room temperature. Isomer shifts (I.S.) were expressed with respect to the centroid of the spectrum of a metallic iron foil. The Doppler velocity was set to ±10.0 mm/s. Gamma rays at 14.4 keV were collected from each sample for 3 or 4 days. The Mössbauer spectra were fitted using a least-squares method with restrictions on the intensity and half width (H.W.) of the peaks. All doublets were treated as symmetric. The relative content (%) of the individual iron species in an analyzed sample was calculated as the peak area in the Mössbauer spectrum.

4. Results

Table 1 lists all of the measurements of the $\delta^{15}N$, $\delta^{13}C_{org}$, and $\delta^{34}S$ values; the TN, TOC, and CRS contents; and the TOC/TN atomic ratios of the samples collected from the study section. Certain TOC values previously reported in Saitoh et al. (2013a) are also shown in Table 1. Fig. 2 shows the chemostratigraphic profiles of the $\delta^{15}N$, $\delta^{34}S$, and $\delta^{13}C_{org}$ values; the TOC, TN, and CRS contents; and the TOC/TN ratios across the G–LB at Chaotian. Fig. 3 shows the geochemical cross-plots of the analyzed samples. The $\delta^{15}N$ values range from +2.7 to +13.9‰, with an average value of +10.1‰. The $\delta^{13}C_{org}$ values range from −30.9 to −24.7‰, with an average value of −27.4‰, and the $\delta^{34}S$ values range from −41.5 to +10.0‰, with an average value of −22.1‰. The TN contents range from 5 to 7235 ppm, with an average value of 1381 ppm, and the TOC contents range from 0.0 to 16.1%, with an average value of 2.6%. The CRS contents range from 16 to 23,891 ppm, with an average value of 4427 ppm, and the TOC/TN ratios range from 6.1 to 68.0, with an average value of 34.9.

Table 2 lists the analytical results of the ^{57}Fe Mössbauer spectroscopic analyses of the rock samples in the Mudstone Unit of the Maokou Formation at Chaotian. Fig. 4a and b shows the representative Mössbauer spectra of the black calcareous mudstone from the Mudstone Unit. Two iron species were identified in the present study: pyrite iron (FeP) and paramagnetic Fe^{2+} (high spin). No ferric oxide (e.g., hematite and magnetite) iron was recognized. Pyrite iron is dominant (>90%) in all of the analyzed samples in the Mudstone Unit. In addition to the rocks in the Mudstone Unit, we preliminarily analyzed bioclastic limestones in the Limestone Unit of the Maokou Formation at Chaotian, but could not detect any Mössbauer spectrum in the shelf limestones due to their low iron contents.

5. Discussion

5.1. Preservation of the original isotopic compositions

Post-depositional processes may have changed the original isotopic compositions in the analyzed rocks at Chaotian. To evaluate the diagenetic imprints, we examined the relationships between the TN, TOC, and CRS contents and the observed isotopic compositions of the analyzed samples (Fig. 3). The TN and TOC contents of the samples are strongly correlated (Fig. 3a), indicating that the main source of nitrogen in the rocks is sedimentary organic matter. A certain amount of organic nitrogen may have been lost during sinking in the water column and/or after burial because the C/N ratios are generally higher than 6.6 (the Redfield value).

Generally, the $\delta^{15}N$ value of the organic matter in the sediments would increase due to a preferential ^{14}N loss during burial and early sedimentary diagenesis, including thermal maturation (e.g., Altabet and Francois, 1994; Williams et al., 1995; Jia and Kerrich, 2004; Robinson et al., 2012); in that case, a negative correlation between the $\delta^{15}N$ value and the TN content in the sedimentary records would be expected (Cremonese et al., 2013). No strong negative correlation between the $\delta^{15}N$ values and the TN contents is observed in the analyzed samples at Chaotian (Fig. 3c), implying that the selective ^{14}N loss after burial is negligible. However, the $\delta^{15}N$ values and the C/N ratios are negatively correlated in the Maokou and Wujiaping Formations (Fig. 3f). The increasing C/N ratios may reflect the increasing diagenetic alteration of the organic matter (Bristow et al., 2009); therefore, the relationship between the $\delta^{15}N$ values and the C/N ratios at Chaotian implies that the diagenesis of the organic matter led to lower $\delta^{15}N$ values. However, the supposed isotopic change appears smaller than the observed stratigraphic variation between the Maokou and Wujiaping Formations; the diagenetic ^{15}N loss cannot explain the systematic difference between the high $\delta^{15}N$ values in the Maokou Formation and the low $\delta^{15}N$ values in the Wujiaping Formation. Even if a certain amount of diagenetic ^{15}N loss may have occurred, it remains likely that the systematic difference in the $\delta^{15}N$ value between the sedimentary units and, particularly, the high $\delta^{15}N$ values in the Mudstone Unit reflects the primary isotopic trends. No positive correlation between the $\delta^{15}N$ and $\delta^{13}C_{org}$ values is observed in the analyzed samples (Fig. 3h). A positive correlation between the $\delta^{15}N$ and $\delta^{13}C_{org}$ values may suggest a preferential loss of ^{14}N and ^{12}C by hydrothermal alteration and/or metamorphic devolatilization (Pinti et al., 2009); this is not likely the case at Chaotian. The C/N ratios are relatively low in the Mudstone Unit of the Maokou Formation at Chaotian (Fig. 2), suggesting that little selective N loss occurred during diagenesis and the primary $\delta^{15}N$ values are preserved in the unit. The Mudstone Unit was deposited under anoxic conditions (Isozaki et al., 2008; Saitoh et al., 2013a), which may have been suitable to preserve the original $\delta^{15}N$ signatures (Altabet et al., 1999; Thomazo et al., 2011). In summary, the observed $\delta^{15}N$ values at Chaotian, including the high values in the Mudstone Unit, likely represent the primary isotopic compositions.

No strong correlation between the $\delta^{13}C_{org}$ value and the TOC content is observed in the analyzed samples (Fig. 3d), suggesting that the preferential ^{12}C loss during degradation is not significant (Hayes et al., 1983; Ueno et al., 2004). A weakly negative correlation is recognized in the black mudstone in the Mudstone Unit, which may reflect selective ^{12}C loss after burial. However, no negative correlation between the $\delta^{13}C_{org}$ value and the TOC content is observed in the dark gray muddy limestone that alternates with the black mudstone in the Mudstone Unit. The $\delta^{13}C_{org}$ value of the dark gray muddy limestone is likely more susceptible to preferential ^{12}C loss than the black mudstone because the TOC contents of the dark gray muddy limestone are systematically lower than those of the black mudstones (Figs. 2 and 3d); no linear correlation between the $\delta^{13}C_{org}$ value and the TOC content in the dark gray muddy limestone implies that the observed weakly

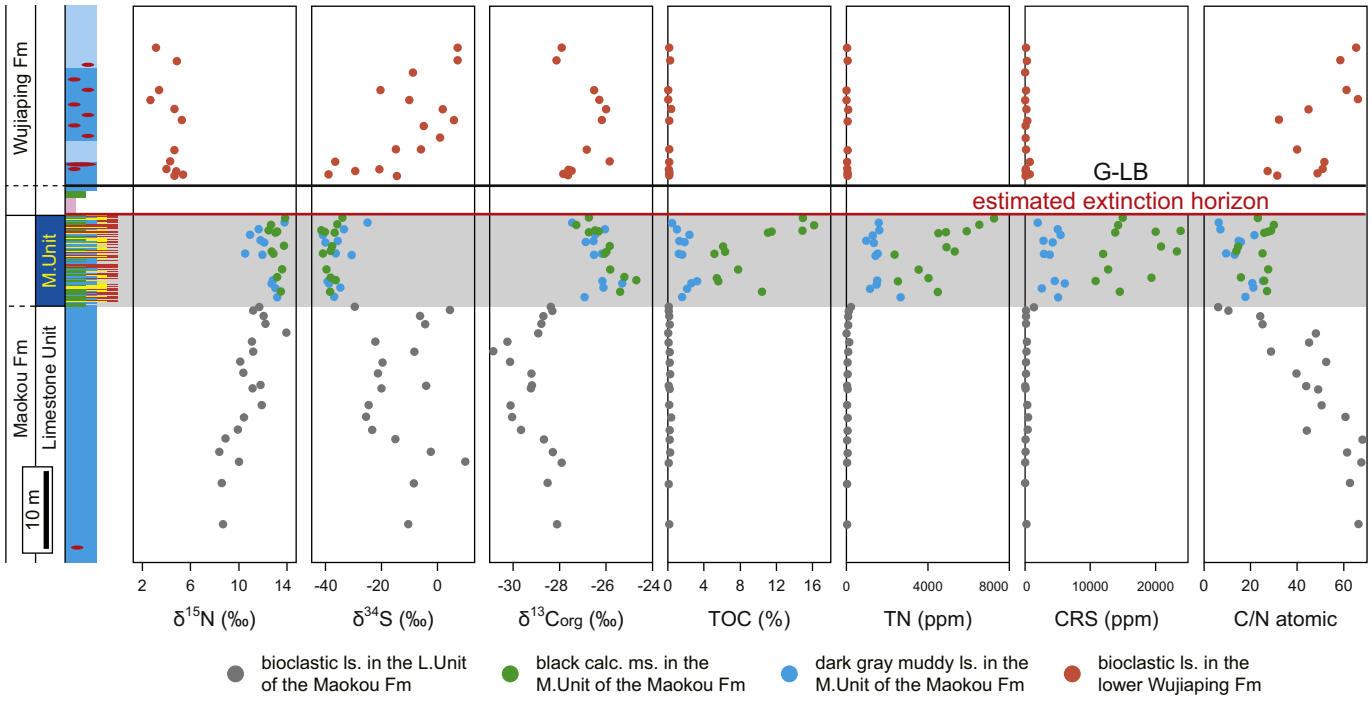

Fig. 2. Chemostratigraphy across the G–LB at Chaotian. Certain TOC values are reported by Saitoh et al. (2013a). ls.: limestone; ms.: mudstone; L.: Limestone; M.: Mudstone; TN: total nitrogen; CRS: chromium(II)-reducible sulfur.

negative correlation in the black mudstones is not a result of diagenetic ^{12}C loss. No positive correlation between the $\delta^{15}N$ and $\delta^{13}C_{org}$ values is observed in the analyzed samples, as noted above (Fig. 3h), suggesting that the diagenetic loss of ^{14}N and ^{12}C may have had only a minor influence on the isotopic compositions (Pinti et al., 2009). A positive correlation between the TOC content and the TOC/TN atomic ratio in the rocks would be expected if selective addition or loss of carbon occurred during diagenesis (e.g., Calvert, 2004). In contrast, if the sediments sustained significant thermal maturation after burial, TOC contents and TOC/TN ratios would decrease and increase, respectively; in that case, a negative correlation between the TOC content and the TOC/TN ratio would be expected (Bristow et al., 2009). No strong correlation between the TOC content and the TOC/TN ratio is observed in the analyzed samples at Chaotian (Fig. 3b), suggesting that the grade of thermal maturity is low.

No correlation between the $\delta^{34}S$ value and the CRS content is observed in the analyzed samples (Fig. 3e). If a preferential loss of heavy/light sulfur occurred after burial, a linear relationship between the $\delta^{34}S$ value and the CRS content would be expected, similar to that in the nitrogen and carbon cases. The observation that there was no correlation at Chaotian suggests that the selective $^{34}S/^{32}S$ loss during diagenesis was not significant and that the observed $\delta^{34}S$ values represent the original isotopic signatures.

5.2. Environmental changes in the disphotic zone at the end-Guadalupian

5.2.1. Water-mass anaerobic respiration

At Chaotian, the $\delta^{15}N$ values increase from +8 to +14‰ in the topmost Maokou Formation and then drop below +6‰ across the G–LB (Fig. 2). The $\delta^{15}N$ value of up to +14‰ in the Mudstone Unit is considerably high in the Phanerozoic (e.g., Kidder and Worsley, 2010). The most plausible explanation for the high $\delta^{15}N$ values is denitrification in the Capitanian ocean, where ^{15}N-rich residual nitrate was assimilated and finally preserved into sedimentary organic matter after isotopic fractionation by denitrification (ca. 25‰) (e.g., Sigman et al., 2009). The denitrification likely occurred in the water column because denitrification within the sediment exhibits little isotope fractionation and cannot explain the $\delta^{15}N$ increase at Chaotian (Brandes and Devol, 2002). Terrestrial plants generally exhibit relatively low $\delta^{15}N$ values and high C/N ratios compared with marine algae (Peters et al., 1978; Meyers, 1994). The systematically low C/N ratios in the Mudstone Unit at Chaotian imply that the high $\delta^{15}N$ values in the Mudstone Unit may also be partly attributed to the decreasing input of terrestrial organic matter due to deepening (Figs. 1c and 2). The $\delta^{15}N$ values significantly decrease below +6‰ across the G–LB, suggesting a decline in the water-mass denitrification and/or enhanced nitrogen fixation producing a ^{15}N-depleted fixed nitrogen pool (0 to −7‰ relative to paleo-atmospheric N_2; e.g., Minagawa and Wada, 1986; Nishizawa et al., 2007; Nishizawa et al., 2014; Zhang et al., 2014), in the aftermath of the end-Guadalupian extinction. The increasing contribution of the terrestrial plants of relatively low $\delta^{15}N$ values after shallowing may be an additional mechanism underlying the lower $\delta^{15}N$ values in the Wujiaping Formation.

The $\delta^{34}S$ values are relatively scattered in the shallow bioclastic limestone of the Limestone Unit of the Maokou Formation and then decrease to consistently low values of approximately −37‰ in the overlying Mudstone Unit of the deep-water facies (Fig. 2). Above the G–LB, the $\delta^{34}S$ values are again scattered from −39 to +7‰ in the Wujiaping bioclastic limestone. Generally, microbial sulfate reduction produced ^{34}S-depleted sulfide because of the large kinetic isotopic effects (e.g., Canfield, 2001a, 2001b). The scattered and high $\delta^{34}S$ values in the shallow marine limestones at Chaotian suggest sulfate reduction in a closed system within the sediments (Jørgensen, 1979). In contrast, the consistently low $\delta^{34}S$ values in the Mudstone Unit indicate that sulfate reduction operated in an open system, most likely within the water column, which was enriched in sulfate (e.g., Wijsman et al., 2001).

The $\delta^{13}C_{org}$ values are relatively low (−31 to −28‰) in the Limestone Unit of the Maokou Formation at Chaotian (Fig. 2). In contrast, the $\delta^{13}C_{org}$ values are high (−28 to −25‰) in the overlying Mudstone Unit. In the lower Wujiaping Formation, the $\delta^{13}C_{org}$ values remain high (−28 to −26‰), although they are slightly lower than those in the Mudstone Unit (Fig. 3h). We interpret the $\delta^{13}C_{org}$ increase across the

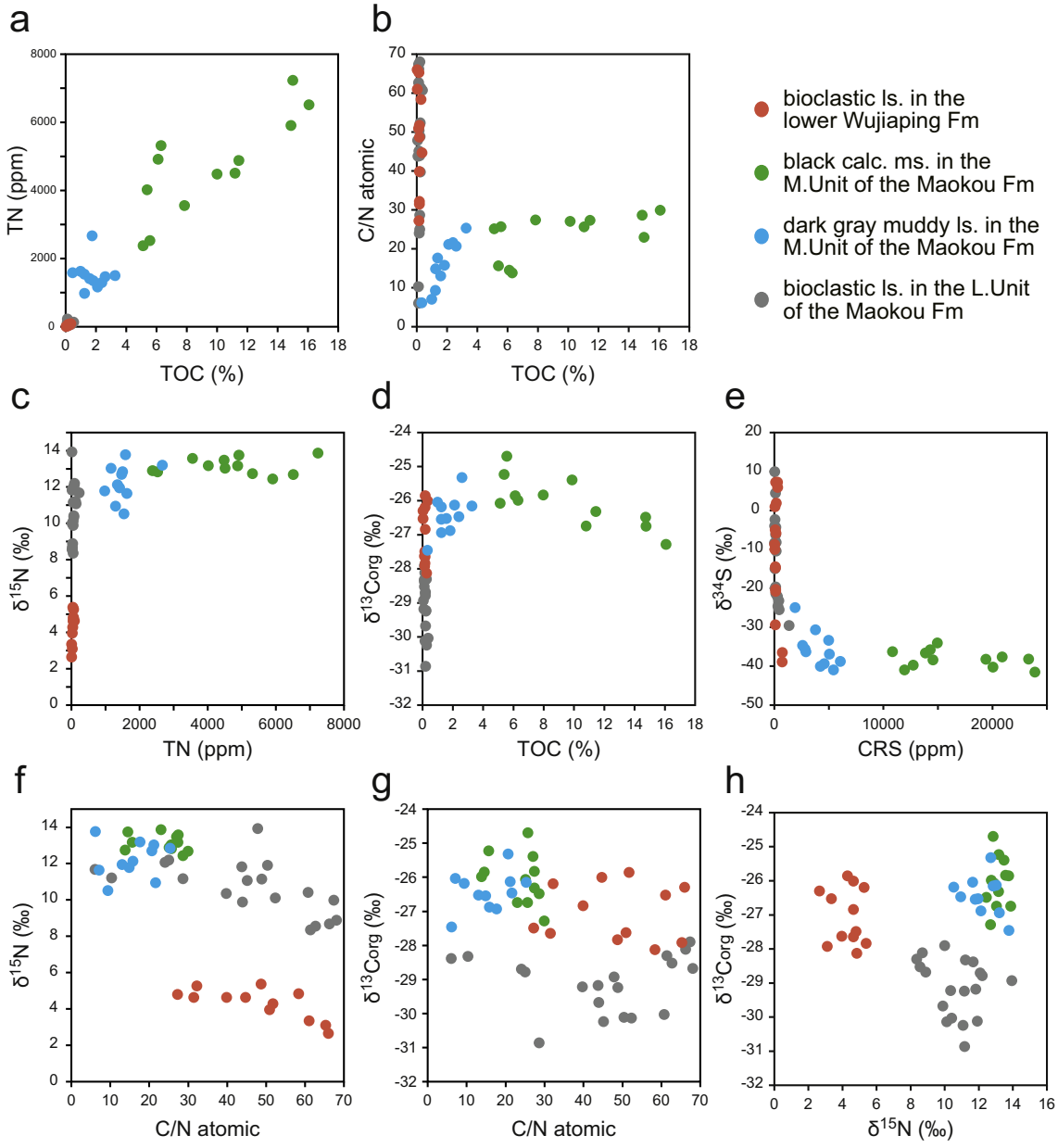

Fig. 3. Geochemical cross-plots of the Guadalupian–Lopingian carbonates at Chaotian. TN vs. TOC (a), C/N vs. TOC (b), $\delta^{15}N$ vs. TN (c), $\delta^{13}C_{org}$ vs. TOC (d), $\delta^{34}S$ vs. CRS (e), $\delta^{15}N$ vs. C/N (f), $\delta^{13}C_{org}$ vs. C/N (g), $\delta^{13}C_{org}$ vs. $\delta^{15}N$ (h).

Limestone/Mudstone unit boundary to be due to the decreasing contribution of the terrestrial plants as a result of deepening because land plants generally exhibit relatively low $\delta^{13}C_{org}$ values compared with marine plankton, particularly in low latitudes (Fig. 1; Sackett and Thompson, 1963; Peters et al., 1978). In land plants, carbon isotopic fractionations in C_4 photosynthesis and in crassulacean acid metabolism (CAM) are relatively small compared with that in C_3 photosynthesis (Bender, 1971; Smith and Epstein, 1971); the $\delta^{13}C_{org}$ values of the C_4 and CAM plants are close to that of marine plankton, complicating an estimation of the sources of the organic matter in the shelf sediments (e.g., Goñi et al., 1997). However, the contributions of C_4 and CAM plants to the sedimentary organic matter may not have been significant in the Paleozoic because it is likely that the C_4 and CAM plants have thrived primarily in the late Mesozoic to Cenozoic (e.g., Sage, 2004; Silvera et al., 2010). The relatively high $\delta^{13}C_{org}$ values in the Mudstone Unit may also be attributed partly to increased primary productivity and enhanced organic carbon burial, implied by the high TOC contents in the unit, and/or increased contribution of organic compounds from green sulfur bacteria of relatively high $\delta^{13}C_{org}$ value (Sirevåg et al., 1977), associated with euxinia in the unit (see Section 5.2.2). In contrast, across the G–LB at Chaotian, the increasing contribution of terrestrial plants as a result of shallowing may have led to slightly lower $\delta^{13}C_{org}$ values in the Wujiaping Formation, although they remain higher than those in the Limestone Unit of the Maokou Formation. The relatively high $\delta^{13}C_{org}$ values in the lower Wujiaping Formation may be partly attributed to the high primary productivity in the surface ocean in the aftermath of the end-Guadalupian extinction. The enhanced nitrogen fixation in the early Wuchiapingian ocean, suggested by the decreased $\delta^{15}N$ values ($<+6‰$), may have promoted the oceanic primary productivity.

Generally, denitrification and sulfate reduction are important biogeochemical pathways under oxygen-depleted conditions (e.g., Jørgensen,

Table 1
Results of nitrogen, organic carbon and sulfur isotope analysis.

Formation/unit	Sample ID	Lithology	Thickness (m)	$\delta^{15}N$ vs. Air-N_2 (‰)	$\delta^{13}C_{org}$ vs. VPDB (‰)	$\delta^{34}S$ vs. VCDT (‰)	TN (ppm)	TOC (%)	CRS (ppm)	TOC/TN atomic
Lower Wujiaping Fm	99W017	Bioclastic limestone	55.6	3.1	−27.9	7.2	25	0.1	116	65.3
Lower Wujiaping Fm	11W8	Bioclastic limestone	54.1	4.8	−28.1	7.3	56	0.3	287	58.3
Lower Wujiaping Fm	11W7	Bioclastic limestone	52.7	–	–	−8.7	–	–	33	–
Lower Wujiaping Fm	11W6.5	Bioclastic limestone	50.6	3.4	−26.5	−20.3	7	0.0	128	61.0
Lower Wujiaping Fm	11W6	Bioclastic limestone	49.5	2.7	−26.3	−10.0	5	0.0	39	66.0
Lower Wujiaping Fm	11W5	Bioclastic limestone	48.4	4.6	−26.0	1.9	89	0.3	187	44.7
Lower Wujiaping Fm	11W4	Bioclastic limestone	47.1	5.3	−26.2	5.9	61	0.2	311	32.2
Lower Wujiaping Fm	11W3	Bioclastic limestone	46.5	–	–	−5.0	–	–	78	–
Lower Wujiaping Fm	11W2	Bioclastic limestone	45.1	–	–	1.0	–	–	57	–
Lower Wujiaping Fm	11W1.5	Bioclastic limestone	43.7	–	–	−14.8	–	–	104	–
Lower Wujiaping Fm	11W1	Bioclastic limestone	43.7	4.6	−26.8	−5.9	50	0.2	158	39.9
Lower Wujiaping Fm	99W13	Bioclastic limestone	42.3	4.3	−25.9	−36.5	39	0.1	734	51.7
Lower Wujiaping Fm	99W6	Bioclastic limestone	41.4	4.0	−27.6	−20.8	28	0.1	115	50.9
Lower Wujiaping Fm	99W5	Bioclastic limestone	41.1	4.8	−27.5	−29.4	62	0.1	97	27.2
Lower Wujiaping Fm	99W3	Bioclastic limestone	40.8	5.4	−27.8	−38.9	41	0.2	720	48.7
Lower Wujiaping Fm	99W2	Bioclastic limestone	40.7	4.6	−27.6	−14.4	64	0.2	96	31.5
Mudstone Unit of Maokou Fm	E72	Black calcareous mudstone	35.7	13.9	−26.7	−34.0	7235	15.2	14,959	23.0
Mudstone Unit of Maokou Fm	E54	Dark gray muddy limestone	35.2	13.8	−27.5	−25.0	1587	0.3	1918	6.2
Mudstone Unit of Maokou Fm	E48	Black calcareous mudstone	34.9	12.7	−27.3	−35.8	6512	16.1	14,300	29.9
Mudstone Unit of Maokou Fm	E31	Dark gray muddy limestone	34.4	11.6	−26.0	−33.4	1627	1.0	4990	7.1
Mudstone Unit of Maokou Fm	E26	Black calcareous mudstone	34.3	12.4	−26.5	−41.5	5908	15.0	23,891	28.6
Mudstone Unit of Maokou Fm	E21	Black calcareous mudstone	34.1	13.2	−26.3	−40.3	4880	11.6	20,044	27.3
Mudstone Unit of Maokou Fm	E13	Black calcareous mudstone	34.0	13.0	−26.7	−36.6	4507	11.3	13,855	25.6
Mudstone Unit of Maokou Fm	E1	Dark gray muddy limestone	33.8	10.9	−26.5	−40.9	1293	2.5	5437	21.6
Mudstone Unit of Maokou Fm	D106	Dark gray muddy limestone	33.1	11.8	−26.5	−35.6	976	1.2	2813	14.9
Mudstone Unit of Maokou Fm	D98	Dark gray muddy limestone	32.9	12.1	−26.9	−40.0	1350	1.7	4221	15.8
Mudstone Unit of Maokou Fm	D85	Black calcareous mudstone	32.4	13.8	−25.9	−37.6	4916	6.4	20,895	14.5
Mudstone Unit of Maokou Fm	D71	Black calcareous mudstone	31.9	12.7	−26.0	−38.2	5313	6.1	23,314	13.8
Mudstone Unit of Maokou Fm	D60	Dark gray muddy limestone	31.6	10.5	−26.2	−36.3	1540	1.0	2909	9.3
Mudstone Unit of Maokou Fm	D59	Black calcareous mudstone	31.6	12.9	−26.1	−41.0	2377	5.0	11,943	25.1
Mudstone Unit of Maokou Fm	D53	Dark gray muddy limestone	31.4	12.0	−26.5	−30.6	1413	1.5	3761	13.0
Mudstone Unit of Maokou Fm	D12	Black calcareous mudstone	29.8	13.6	−25.8	−39.7	3555	7.9	12,740	27.4
Mudstone Unit of Maokou Fm	C62	Black calcareous mudstone	28.8	13.2	−25.2	−38.2	4019	5.8	19,398	15.6
Mudstone Unit of Maokou Fm	C55	Black calcareous mudstone	28.4	12.8	−24.7	−36.3	2528	5.5	10,836	25.7
Mudstone Unit of Maokou Fm	C54	Dark gray muddy limestone	28.4	12.8	−26.2	−39.3	1500	3.2	4553	25.3
Mudstone Unit of Maokou Fm	C43	Dark gray muddy limestone	28.1	12.7	−25.3	−38.8	1471	2.5	6060	20.7
Mudstone Unit of Maokou Fm	C28	Dark gray muddy limestone	27.6	13.0	−26.1	−34.7	1164	2.1	2586	21.1
Mudstone Unit of Maokou Fm	C10	Black calcareous mudstone	27.1	13.5	−25.4	−38.4	4481	10.1	14,557	27.0
Mudstone Unit of Maokou Fm	B16	Dark gray muddy limestone	26.5	13.2	−26.9	−36.9	2667	1.7	5066	17.7
Limestone Unit of Maokou Fm	07MU31	Bioclastic limestone	25.4	11.7	−28.4	−29.5	225	0.1	1339	6.1
Limestone Unit of Maokou Fm	07MU29	Bioclastic limestone	24.9	11.2	−28.3	4.4	119	0.1	106	10.3
Limestone Unit of Maokou Fm	07MU25	Bioclastic limestone	24.3	12.1	−28.7	−6.2	79	0.2	122	24.0
Limestone Unit of Maokou Fm	07MU22	Bioclastic limestone	23.4	12.2	−28.8	−4.3	90	0.2	138	25.0
Limestone Unit of Maokou Fm	07MU19	Bioclastic limestone	22.3	13.9	−28.9	–	15	0.1	–	47.8
Limestone Unit of Maokou Fm	07MU16	Bioclastic limestone	21.3	11.1	−30.2	−22.1	135	0.1	291	45.1
Limestone Unit of Maokou Fm	07MU12	Bioclastic limestone	20.1	11.2	−30.9	−8.2	81	0.2	173	28.6
Limestone Unit of Maokou Fm	07MU8	Bioclastic limestone	18.9	10.1	−30.1	−19.6	49	0.2	129	52.3
Limestone Unit of Maokou Fm	07MU4	Bioclastic limestone	17.6	10.3	−29.2	−21.3	70	0.2	130	39.7
Limestone Unit of Maokou Fm	07MU2	Bioclastic limestone	16.2	11.8	−29.2	−4.0	22	0.1	24	43.8
Limestone Unit of Maokou Fm	07MU1	Bioclastic limestone	15.8	11.2	−29.2	−20.0	54	0.2	73	48.8
Limestone Unit of Maokou Fm	03Mao17	Bioclastic limestone	13.9	11.9	−30.1	−24.6	36	0.2	323	50.4
Limestone Unit of Maokou Fm	03Mao16	Bioclastic limestone	12.5	10.4	−30.0	−25.5	71	0.4	449	60.7
Limestone Unit of Maokou Fm	03Mao15	Bioclastic limestone	11.0	9.9	−29.7	−23.2	52	0.2	408	43.9
Limestone Unit of Maokou Fm	03Mao14	Bioclastic limestone	9.9	8.9	−28.7	−15.0	35	0.2	64	68.0
Limestone Unit of Maokou Fm	03Mao13	Bioclastic limestone	8.4	8.4	−28.3	−2.3	49	0.3	55	61.4
Limestone Unit of Maokou Fm	03Mao12	Bioclastic limestone	7.2	10.0	−27.9	10.0	21	0.1	28	67.4
Limestone Unit of Maokou Fm	03Mao11	Bioclastic limestone	4.8	8.6	−28.5	−8.4	22	0.1	16	62.7
Limestone Unit of Maokou Fm	03Mao9	Bioclastic limestone	0.0	8.7	−28.1	−10.4	25	0.1	174	66.2

1982; Codispoti and Christensen, 1985). The enhanced anaerobic respiration in the Mudstone Unit at Chaotian is consistent with the oxygen depletion in the unit that was suggested by the characteristics of the litho- and bio-facies (Isozaki et al., 2008; Saitoh et al., 2013a) (Fig. 1c). Moreover, the present nitrogen and sulfur isotopic results at Chaotian indicate that the oxygen depletion was not restricted within the sediments but, rather, prevailed in the water column in the disphotic zone in the Capitanian oceans, promoting water-mass anaerobic respiration.

5.2.2. Emergence of a sulfidic water mass

The enhanced sulfate reduction in the anoxic water column, based on the $\delta^{34}S$ records of the Mudstone Unit at Chaotian, may have caused the accumulation of hydrogen sulfide on the disphotic slope/basin, resulting in the emergence of a sulfidic deep-water mass (Fig. 5). The pyrite framboids of relatively small size (mostly 5–7 μm in diameter) occur abundantly throughout the Mudstone Unit (Saitoh et al., 2013a), and it is compatible with the emergence of the sulfidic water mass (Wilkin et al., 1996). To investigate the redox conditions of the Mudstone Unit in more detail, we analyzed the chemical states of the iron in the rock samples. Iron speciation in rock samples is useful to reconstruct the redox conditions of the sedimentary environments (Raiswell and Canfield, 1998; Poulton and Canfield, 2005), and, in particular, the ratio of the chemically highly reactive iron to total iron (FeHR/FeT) and the proportion of FeHR bound as the sulfide phase

Table 2
Results of ^{57}Fe Mössbauer spectroscopic analysis. I.S.: isomer shifts, Q.S.: quadrupole splitting, H.W.: half width.

Formation/unit	Sample ID	Lithology	Thickness (m)	Fe species	Peak area (%)	I.S. (mm/s)	Q.S. (mm/s)	H.W. (mm/s)
Mudstone Unit of Maokou Fm	E72	Black calcareous mudstone	35.7	Pyrite	92.4	0.318	0.607	0.285
				Fe^{2+} (high spin)	7.6	1.173	2.672	0.512
Mudstone Unit of Maokou Fm	E48	Black calcareous mudstone	34.9	Pyrite	100.0	0.311	0.591	0.284
Mudstone Unit of Maokou Fm	E31	Dark gray muddy limestone	34.4	Pyrite	100.0	0.295	0.572	0.249
Mudstone Unit of Maokou Fm	E26	Black calcareous mudstone	34.3	Pyrite	100.0	0.304	0.603	0.285
Mudstone Unit of Maokou Fm	E21	Black calcareous mudstone	34.1	Pyrite	100.0	0.304	0.607	0.291
Mudstone Unit of Maokou Fm	E13	Black calcareous mudstone	34.0	Pyrite	100.0	0.305	0.602	0.287
Mudstone Unit of Maokou Fm	E1	Dark gray muddy limestone	33.8	Pyrite	100.0	0.303	0.599	0.292
Mudstone Unit of Maokou Fm	D85	Black calcareous mudstone	32.4	Pyrite	100.0	0.303	0.603	0.291
Mudstone Unit of Maokou Fm	D71	Black calcareous mudstone	31.9	Pyrite	100.0	0.304	0.601	0.291
Mudstone Unit of Maokou Fm	D59	Black calcareous mudstone	31.6	Pyrite	100.0	0.300	0.602	0.284
Mudstone Unit of Maokou Fm	D53	Dark gray muddy limestone	31.4	Pyrite	100.0	0.309	0.647	0.328
Mudstone Unit of Maokou Fm	D12	Black calcareous mudstone	29.8	Pyrite	100.0	0.308	0.597	0.289
Mudstone Unit of Maokou Fm	C62	Black calcareous mudstone	28.8	Pyrite	91.5	0.31	0.604	0.297
				Fe^{2+} (high spin)	8.5	1.144	2.794	0.614
Mudstone Unit of Maokou Fm	C55	Black calcareous mudstone	28.4	Pyrite	100.0	0.300	0.588	0.300
Mudstone Unit of Maokou Fm	C43	Dark gray muddy limestone	28.1	Pyrite	100.0	0.295	0.579	0.311
Mudstone Unit of Maokou Fm	C10	Black calcareous mudstone	27.1	Pyrite	100.0	0.300	0.592	0.295
Mudstone Unit of Maokou Fm	B16	Dark gray muddy limestone	26.5	Pyrite	100.0	0.302	0.609	0.271

(FeP/FeHR) are robust redox indicators of past oceans (e.g., Canfield et al., 2007, 2008). FeHR was originally defined as the sum of the dithionite-extractable iron and FeP (Raiswell and Canfield, 1998), although the definition has been slightly modified to the sum of iron oxide, carbonate, and sulfide minerals, after Poulton and Canfield (2005). The degree of pyritization (DOP) was defined as the ratio of FeP to the sum of FeP and HCl-extractable Fe as an indicator of a euxinic condition (Berner, 1970; Raiswell et al., 1988). Because HCl-extractable Fe includes a certain amount of iron from sheet silicates, the DOP has recently tended to be replaced by FeP/FeHR (e.g., Canfield et al., 2008; Reinhard et al., 2009). When the FeHR/FeT and FeP/FeHR ratios of a sample are greater than 0.38 and 0.8, respectively, the deposition under sulfidic conditions is indicated based on the analyses of modern marine sediments from various locations worldwide (Raiswell and Canfield, 1998).

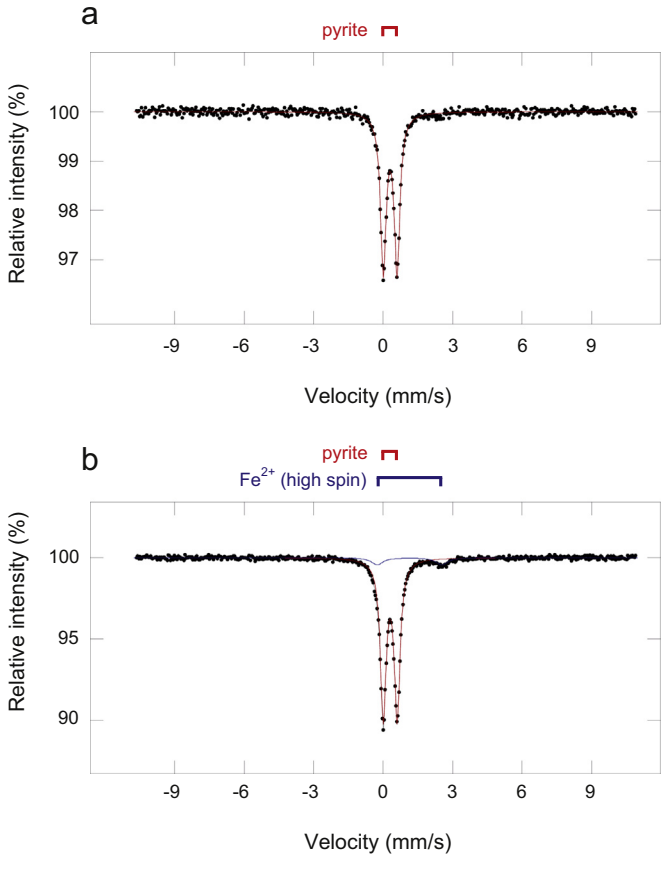

Fig. 4. Representative Mössbauer spectra of black calcareous mudstone in the Mudstone Unit at Chaotian. The spectra are of D12 (a) and C62 (b), respectively. A fitting curve of pyrite is expressed in red. The clear doublet peak shows that pyrite Fe is dominant in both samples. In b, a minor component of paramagnetic Fe^{2+} (high spin) (the fitting curve is in blue) is also detected. (For interpretation of the references to color in this figure legend, the reader is referred to the web version of this article.)

In the present study, the iron speciation of the sedimentary rocks of the Mudstone Unit at Chaotian was examined by ^{57}Fe Mössbauer spectroscopy (Matsuo et al., 2003). The present results show that pyrite Fe is dominant in all of the analyzed samples, and the FeP/FeT ratio is consistently greater than 0.9 in the Mudstone Unit (Fig. 4a,b; Table 2). Generally, the FeHR/FeT and FeP/FeHR ratios are consistently higher than the FeP/FeT ratio because FeHR is higher than FeP and lower than FeT. The present ^{57}Fe Mössbauer spectroscopic results at Chaotian show that the FeHR/FeT and FeP/FeHR ratios are greater than 0.9 throughout the Mudstone Unit, indicating that the unit was deposited under sulfidic conditions.

5.2.3. Possible relationship with the deep-sea anoxia and the shallow-sea extinction

It should be considered whether the development of anoxic/sulfidic waters in the Capitanian oceans was a regional event around Chaotian in the eastern Tethys or was a global phenomenon (Fig. 1b). Yan et al. (2013) recently suggested the development of anoxic deep-water corresponding to the end-Guadalupian extinction at Tieqiao in Guangxi, South China, based on the sulfur isotope records of carbonate-associated sulfate. Schoepfer et al. (2012) reported high δ^{15}N values (up to +10‰) in the Middle Permian Ranger Canyon Formation at the Opal Creek section in southwestern Alberta, Canada (Fig. 1b); the high δ^{15}N values imply denitrification in the mid-water oxygen minimum zone in the Capitanian. The presence of the anoxic water in the Middle Permian at Opal Creek was also supported by sulfide sulfur isotope records and trace element enrichments (Schoepfer et al., 2013). During the Permian, Opal Creek was located on the northwestern margin of Pangea and on the opposite side of the globe from Chaotian (and Tieqiao) in South China (Fig. 1b). Although an extensive unconformity across the G–LB (ranging over 5–7 million years) and the thin Middle-Upper Permian strata (less than 4 m thick in total) at Opal Creek prevent an exact correlation with the present results at Chaotian (Schoepfer et al., 2012, 2013), the previous and present results suggest that the anoxic/sulfidic deep-water masses in which the anaerobic respiration

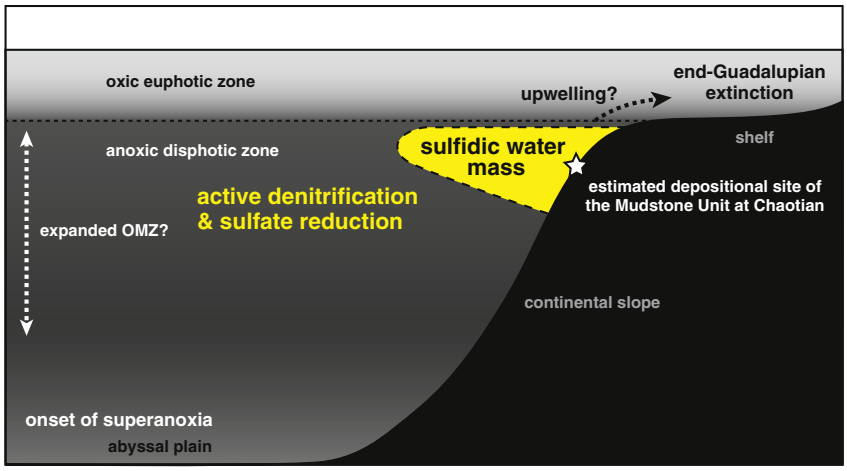

Fig. 5. Schematic diagram of the environmental changes in the oceans at the end-Guadalupian proposed in this study. An expansion of the oxygen minimum zone (OMZ) caused by the increased primary productivity in the surface oceans enhanced the anaerobic respiration in the relatively deep disphotic zone. The active water-mass sulfate reduction resulted in the emergence of a sulfidic deep-water mass in the disphotic zone at the continental margin. The OMZ expansion corresponded to the onset of the prolonged oxygen depletion in the deep sea. An upwelling of the sulfidic deep-water from the disphotic zone to the shallow shelves along the continental margin stressed the shallow-marine biota.

was enhanced were widespread in the Capitanian oceans on a global scale.

Because the disphotic zone is between the shallow- and deep-sea areas in the oceans, the environmental changes in the disphotic zone at the end-Guadalupian suggested in this study might have been associated with the onset of deep-sea oxygen depletion and the shallow-sea extinction (Fig. 5). The water-mass anaerobic respiration in the disphotic zone suggested by the present results at Chaotian was possibly enhanced by an expansion of the oxygen minimum zone (OMZ) in the oceans because anaerobic respiration is generally promoted under oxygen-depleted conditions. The increased primary productivity in the surface oceans and the enhanced biological pumps in the Capitanian, suggested by the high $\delta^{13}C_{carb}$ values of the shelf carbonates on a global scale named the "Kamura event" (Isozaki et al., 2007, 2011), may have expanded the OMZ. Additionally, the expansion of the OMZ at the end-Guadalupian might have corresponded to the onset of the prolonged oxygen depletion in the deep sea around the G–LB (Isozaki, 1997), although the details of the deep-ocean redox conditions during the late Permian remain a topic of discussion (Algeo et al., 2010; Wignall et al., 2010).

The bio- and chemo-stratigraphic relationships across the G–LB at Chaotian clearly indicate that the sulfidic deep-water mass emerged on the disphotic slope/basin prior to the end-Guadalupian extinction on the shallow shelves (Figs. 1 and 2; Saitoh et al., 2013a). This stratigraphic relationship implies that the sulfidic deep-waters have possibly acted as a stress to the shallow-marine biota by upwelling along the continental margin, as suggested by the $\delta^{13}C_{carb}$ records at Chaotian (Fig. 5; Saitoh et al., 2013b). During the Permian, Chaotian was located on the western side of South China and most likely faced the eastern Paleo-Tethys around the equator; the location may have been suitable for an upwelling caused by the trade winds, as observed in the modern oceans. Moreover, the fossil records have demonstrated that benthic invertebrates, such as brachiopods, fusulines, and rugose corals, were eliminated on a large scale during the end-Guadalupian extinction (e.g., Stanley and Yang, 1994; Clapham et al., 2009); these taxa are generally susceptible to hydrogen sulfide and the extinction pattern is compatible with the upwelling scenario. The eruption of the Emeishan flood basalts in South China has been regarded as a major candidate for the cause of the extinction because the timing of the eruption corresponds with that of the extinction (e.g., Zhou et al., 2002; Wignall et al., 2009; Bond et al., 2010). Although the present results at Chaotian do not exclude other factors, including the eruption of the Emeishan flood basalts, as the cause of the shelf extinction, the sulfidic deep-waters in the disphotic zone may also have contributed to the environmental deterioration on the shallow shelves by the upwelling along the continental margin at the end-Guadalupian. The influence of the sulfidic deep-water to the shelf extinction can be evaluated by further stratigraphic studies across the G–LB in various sections around the world, particularly focusing on the previously overlooked disphotic zone in the oceans.

6. Conclusions

To examine the environmental changes in the relatively deep disphotic zone in the ocean at the end-Guadalupian (Middle Permian), focusing on their possible relationships with the deep-sea oxygen depletion and the shallow-sea extinction, the nitrogen and sulfur isotope geochemistry of the Guadalupian–Lopingian (Upper Permian) shelf carbonates were analyzed at Chaotian in northern Sichuan, South China. Moreover, the chemical states of the iron in the rocks were analyzed by ^{57}Fe Mössbauer spectroscopy to investigate the redox conditions on the disphotic slope/basin in northwestern South China at the end-Guadalupian. The following new results were obtained:

1. Substantially high $\delta^{15}N$ values of total nitrogen (up to +14‰) and consistently low $\delta^{34}S$ values of pyrite (ca. −37‰) in the topmost Maokou Formation, immediately below the Guadalupian–Lopingian boundary, indicate water-column denitrification and sulfate reduction, respectively, in the previously overlooked disphotic zone in the Capitanian (Late Guadalupian) oceans.
2. The enhanced water-mass sulfate reduction likely resulted in the emergence of a sulfidic deep-water mass on the disphotic slope/basin at Chaotian, which is supported by the high proportions of pyrite Fe to highly reactive Fe in the sedimentary rocks.
3. An expansion of the oxygen minimum zone (OMZ) caused by the increased primary productivity in the surface oceans in the Capitanian may have enhanced the anaerobic respiration in the disphotic zone; the OMZ expansion may also have corresponded to the onset of deep-sea oxygen depletion. An upwelling of the sulfidic deep-water from the disphotic zone to the shallow shelves along the continental margin might have stressed the shallow-marine biota at the end-Guadalupian.

Acknowledgments

This study was supported by JSPS KAKENHI (16204040, 20224012, 22310006, 26610159) and CGS (1212011120116, 1212011120143). Y.U. is supported by the NEXT program of JSPS. Two anonymous reviewers gave us constructive comments to improve the manuscript. M. Nakagawa assisted with the S isotope analysis.

References

Algeo, T.J., Hinnov, L., Moser, J., Maynard, J.B., Elswick, E., Kuwahara, K., Sano, H., 2010. Changes in productivity and redox conditions in the Panthalassic Ocean during the latest Permian. Geology 38, 187–190.

Altabet, M.A., Francois, R., 1994. Sedimentary nitrogen isotopic ratio as a recorder for surface ocean nitrate utilization. Glob. Biogeochem. Cycles 8, 103–116.

Altabet, M.A., Pilskaln, C., Thunell, R., Pride, C., Sigman, D., Chavez, F., Francois, R., 1999. The nitrogen isotope biogeochemistry of sinking particles from the margin of the Eastern North Pacific. Deep-Sea Res. I 46, 655–679.

Bender, M.M., 1971. Variations in the $^{13}C/^{12}C$ ratios of plants in relation to the pathway of photosynthetic carbon dioxide fixation. Phytochemistry 10, 1239–1244.

Berner, R.A., 1970. Sedimentary pyrite formation. Am. J. Sci. 268, 1–23.

Bond, D.P.G., Hilton, J., Wignall, P.B., Ali, J.R., Stevens, L.G., Sun, Y.D., Lai, X.L., 2010. The Middle Permian (Capitanian) mass extinction on land and in the oceans. Earth Sci. Rev. 102, 100–116.

Brandes, J.A., Devol, A.H., 2002. A global marine-fixed nitrogen isotopic budget: implications for Holocene nitrogen cycling. Glob. Biogeochem. Cycles 16, 1120.

Bristow, T.F., Kennedy, M.J., Derkowski, A., Droser, M.L., Jiang, G.Q., Creaser, R.A., 2009. Mineralogical constraints on the paleoenvironments of the Ediacaran Doushantuo Formation. Proc. Natl. Acad. Sci. U. S. A. 106, 13190–13195.

Calvert, S.E., 2004. Beware intercepts: interpreting compositional ratios in multicomponent sediments and sedimentary rocks. Org. Geochem. 35, 981–987.

Canfield, D.E., 2001a. Biogeochemistry of sulfur isotopes. In: Valley, J.W., Cole, D.R. (Eds.), Reviews in Mineralogy and Geochemistry. The Mineralogical Society of America, Blacksburg, pp. 607–636.

Canfield, D.E., 2001b. Isotope fractionation by natural populations of sulfate-reducing bacteria. Geochim. Cosmochim. Acta 65, 1117–1124.

Canfield, D.E., Raiswell, R., Westrich, J.T., Reaves, C.M., Berner, R.A., 1986. The use of chromium reduction in the analysis of reduced inorganic sulfur in sediments and shales. Chem. Geol. 54, 149–155.

Canfield, D.E., Poulton, S.W., Narbonne, G.M., 2007. Late-Neoproterozoic deep-ocean oxygenation and the rise of animal life. Science 315, 92–95.

Canfield, D.E., Poulton, S.W., Knoll, A.H., Narbonne, G.M., Ross, G., Goldberg, T., Strauss, H., 2008. Ferruginous conditions dominated later Neoproterozoic deep-water chemistry. Science 321, 949–952.

Chung, S.L., Jahn, B.M., 1995. Plume-lithosphere interaction in generation of the Emeishan flood basalts at the Permian–Triassic boundary. Geology 23, 889–892.

Clapham, M.E., Shen, S.Z., Bottjer, D.J., 2009. The double mass extinction revisited: reassessing the severity, selectivity, and causes of the end-Guadalupian biotic crisis (Late Permian). Paleobiology 35 (1), 32–50.

Codispoti, L.A., Christensen, J.P., 1985. Nitrification, denitrification and nitrous oxide cycling in the eastern tropical North Pacific ocean. Mar. Chem. 16, 277–300.

Cremonese, L., Shields-Zhou, G., Struck, U., Ling, H.F., Och, L., Chen, X., Li, D., 2013. Marine biogeochemical cycling during the early Cambrian constrained by a nitrogen and organic carbon isotope study of the Xiaotan section, South China. Precambrian Res. 225, 148–165.

Goñi, M.A., Ruttenberg, K.C., Eglinton, T.I., 1997. Sources and contribution of terrigenous organic carbon to surface sediments in the Gulf of Mexico. Nature 389, 275–278.

Gradstein, F.M., Ogg, J.G., Schmitz, M.D., Ogg, G., 2012. The Geologic Time Scale 2012. Elsevier, Boston.

Haq, B.U., Schutter, S.R., 2008. A chronology of Paleozoic sea-level changes. Science 322, 64–68.

Hayes, J.M., Kaplan, I.R., Wedeking, K.W., 1983. Precambrian organic geochemistry, preservation of the record. In: Schopf, J.W. (Ed.), Earth's Earliest Biosphere. Princeton Univ. Press, Princeton, pp. 93–134.

Hsieh, Y.P., Shieh, Y.N., 1997. Analysis of reduced inorganic sulfur by diffusion methods: improved apparatus and evaluation for sulfur isotopic studies. Chem. Geol. 137, 255–261.

Irving, E., Parry, L.G., 1963. The magnetism of some Permian rocks from New South Wales. Geophys. J. R. Astron. Soc. 7, 395–411.

Isozaki, Y., 1997. Permo-Triassic boundary Superanoxia and stratified superocean: records from lost deep-sea. Science 276, 235–238.

Isozaki, Y., 2009a. Integrated "plume winter" scenario for the double-phased extinction during the Paleozoic–Mesozoic transition: the G–LB and P–TB events from a Panthalassan perspective. J. Asian Earth Sci. 36, 459–480.

Isozaki, Y., 2009b. Illawarra Reversal: the fingerprint of a superplume that triggered Pangean breakup and the end-Guadalupian (Permian) mass extinction. Gondwana Res. 15, 421–432.

Isozaki, Y., Yao, J.X., Matsuda, T., Sakai, H., Ji, Z.S., Shimizu, N., Kobayashi, N., Kawahata, H., Nishi, H., Takano, M., Kubo, T., 2004. Stratigraphy of the Middle-Upper Permian and Lowermost Triassic at Chaotian, Sichuan, China. Record of Late Permian double mass extinction event. Proc. Jpn. Acad. Ser. B 80, 10–16.

Isozaki, Y., Kawahata, H., Minoshima, K., 2007. The Capitanian (Permian) Kamura cooling event: the beginning of the Paleozoic–Mesozoic transition. Palaeoworld 16, 16–30.

Isozaki, Y., Yao, J.X., Ji, Z.S., Saitoh, M., Kobayashi, N., Sakai, H., 2008. Rapid sea-level change in the Late Guadalupian (Permian) on the Tethyan side of South China: litho- and biostratigraphy of the Chaotian section in Sichuan. Proc. Jpn. Acad. Ser. B 84, 344–353.

Isozaki, Y., Aljinovic, D., Kawahata, H., 2011. The Guadalupian (Permian) Kamura event in European Tethys. Palaeogeogr. Palaeoclimatol. Palaeoecol. 308, 12–21.

Jia, Y., Kerrich, R., 2004. Nitrogen 15-enriched Precambrian kerogen and hydrothermal systems. Geochem. Geophys. Geosyst. 5, Q07005.

Jin, Y.G., Zhang, J., Shang, Q.H., 1994. Two phases of the end-Permian mass extinction. In: Embry, A.F., Beauchamp, B., Glass, D.J. (Eds.), Pangea: Global Environments and Resources. Memoir Canadian Society of Petroleum Geologists vol. 17, pp. 813–822.

Jin, Y.G., Mei, S.L., Wang, W., Wang, X.D., Shen, S.Z., Shang, Q.H., Chen, Z.Q., 1998. On the Lopingian series of the Permian system. Palaeoworld 9, 1–18.

Jørgensen, B.B., 1979. A theoretical model of the stable sulfur isotope distribution in marine sediments. Geochim. Cosmochim. Acta 43, 363–374.

Jørgensen, B.B., 1982. Mineralization of organic matter in the sea bed—the role of sulphate reduction. Nature 296, 643–645.

Jost, A.B., Mundil, R., He, B., Brown, S.T., Altiner, D., Sun, Y.D., DePaolo, D.J., Payne, J.L., 2014. Constraining the cause of the end-Guadalupian extinction with coupled records of carbon and calcium isotopes. Earth Planet. Sci. Lett. 396, 201–212.

Kani, T., Fukui, M., Isozaki, Y., Nohda, S., 2008. The Paleozoic minimum of $^{87}Sr/^{86}Sr$ initial ratio in the upper Guadalupian (Permian) mid-oceanic carbonates: a critical turning point in the Late Paleozoic. J. Asian Earth Sci. 32, 22–33.

Kato, Y., Nakao, K., Isozaki, Y., 2002. Geochemistry of Late Permian to Early Triassic pelagic cherts from southwest Japan: implications for an oceanic redox change. Chem. Geol. 182, 15–34.

Kidder, D.L., Worsley, T.R., 2010. Phanerozoic Large Igneous Provinces (LIPs), HEATT (Haline Euxinic Acidic Thermal Transgression) episodes, and mass extinctions. Palaeogeogr. Palaeoclimatol. Palaeoecol. 295, 162–191.

Lai, X.L., Wang, W., Wignall, P.B., Bond, D.P.G., Jiang, H.S., Ali, J.R., John, E.H., Sun, Y.D., 2008. Palaeoenvironmental change during the end-Guadalupian (Permian) mass extinction in Sichuan, China. Palaeogeogr. Palaeoclimatol. Palaeoecol. 269, 78–93.

Matsuo, M., Kubo, K., Isozaki, Y., 2003. Mössbauer spectroscopic study on characterization of iron in the Permian to Triassic deep-sea chert from Japan. Hyperfine Interact. (C) 5, 435–438.

Meyers, P.A., 1994. Preservation of elemental and isotopic source identification of sedimentary organic matter. Chem. Geol. 114, 289–302.

Minagawa, M., Wada, E., 1986. Nitrogen isotope ratios of red tide organisms in the East-China-Sea—a characterization of biological nitrogen-fixation. Mar. Chem. 19, 245–259.

Nishizawa, M., Sano, Y., Ueno, Y., Maruyama, S., 2007. Speciation and isotope ratios of nitrogen in fluid inclusions from seafloor hydrothermal deposits at 3.5 Ga. Earth Planet. Sci. Lett. 254, 332–344.

Nishizawa, M., Miyazaki, J., Makabe, A., Koba, K., Takai, K., 2014. Physiological and isotopic characteristics of nitrogen fixation by hyperthermophilic methanogens: key insights into nitrogen anabolism of the microbial communities in Archean hydrothermal systems. Geochim. Cosmochim. Acta 138, 117–135.

Peters, K.E., Sweeney, R.E., Kaplan, I.R., 1978. Correlation of carbon and nitrogen stable isotope ratios in sedimentary organic matter. Limnol. Oceanogr. 23, 598–604.

Pinti, D.L., Hashizume, K., Sugihara, A., Massault, M., Philippot, P., 2009. Isotopic fractionation of nitrogen and carbon in Paleoarchean cherts from Pilbara craton, Western Australia: origin of ^{15}N-depleted nitrogen. Geochim. Cosmochim. Acta 73, 3819–3848.

Poulton, S.W., Canfield, D.E., 2005. Development of a sequential extraction procedure for iron: implications for iron partitioning in continentally derived particulates. Chem. Geol. 214, 209–221.

Raiswell, R., Canfield, D.E., 1998. Sources of iron for pyrite formation in marine sediments. Am. J. Sci. 298, 219–245.

Raiswell, R., Buckley, F., Berner, R.A., Anderson, T.F., 1988. Degree of pyritization of iron as a paleoenvironmental indicator of bottom-water oxygenation. J. Sediment. Petrol. 58, 812–819.

Reinhard, C.T., Raiswell, R., Scott, C., Anbar, A.D., Lyons, T.W., 2009. A late Archean sulfidic sea stimulated by early oxidative weathering of the continents. Science 326, 713–716.

Robinson, R.S., Kienast, M., Albuquerque, A.L., Altabet, M., Contreras, S., Holz, R.D.P., Dubois, N., Francois, R., Galbraith, E., Hsu, T.C., Ivanochko, T., Jaccard, S., Kao, S.J., Kiefer, T., Kienast, S., Lehmann, M.F., Martinez, P., McCarthy, M., Mobius, J., Pederson, T., Quan, T.M., Ryabenko, E., Schmittner, A., Schneider, R., Schneider-Mor, A., Shigemitsu, M., Sinclair, D., Somes, C., Studer, A., Thunell, R., Yang, J.Y., 2012. A review of nitrogen isotopic alteration in marine sediments. Paleoceanography 27, PA4203.

Sackett, W.M., Thompson, R.R., 1963. Isotopic organic carbon composition of recent continental derived clastic sediments of eastern Gulf Coast, Gulf of Mexico. AAPG Bull. 47, 525–528.

Sage, R.F., 2004. The evolution of C_4 photosynthesis. New Phytol. 161, 341–370.

Saitoh, M., Isozaki, Y., Yao, J.X., Ji, Z.S., Ueno, Y., Yoshida, N., 2013a. The appearance of an oxygen-depleted condition on the Capitanian disphotic slope/basin in South China: Middle-Upper Permian stratigraphy at Chaotian in northern Sichuan. Glob. Planet. Chang. 105, 180–192.

Saitoh, M., Isozaki, Y., Ueno, Y., Yoshida, N., Yao, J.X., Ji, Z.S., 2013b. Middle-Upper Permian carbon isotope stratigraphy at Chaotian, South China: pre-extinction multiple upwelling of oxygen-depleted water onto continental shelf. J. Asian Earth Sci. 67–68, 51–62.

Sato, T., Isozaki, Y., Shozugawa, K., Matsuo, M., 2011. ^{57}Fe Mössbauer spectroscopic analysis of deep-sea pelagic chert: effect of secondary alteration with respect to paleo-redox evaluation. J. Asian Earth Sci. 42, 1403–1410.

Schoepfer, S.D., Henderson, C.M., Garrison, G.H., Ward, P.D., 2012. Cessation of a productive coastal upwelling system in the Panthalassic Ocean at the Permian–Triassic boundary. Palaeogeogr. Palaeoclimatol. Palaeoecol. 313–314, 181–188.

Schoepfer, S.D., Henderson, C.M., Garrison, G.H., Foriel, J., Ward, P.D., Selby, D., Hower, J.C., Algeo, T.J., Shen, Y.N., 2013. Termination of a continent-margin upwelling system at the Permian–Triassic boundary (Opal Creek, Alberta, Canada). Glob. Planet. Chang. 105, 21–35.

Scotese, C.R., Langford, R.P., 1995. Pangea and the paleogeography of the Permian. In: Scholle, A., Peryt, T.M., Ulmer-Scholle, D.A. (Eds.), The Permian of Northern Pangea vol. 1. Springer, Berlin, pp. 3–19.

Sigman, D.M., Karsh, K.L., Casciotti, K.L., 2009. Ocean process tracers: nitrogen isotopes in the ocean, In: Steele, J.H., Turekian, K.K., Thorpe, S.A. (Eds.), Encyclopedia of Ocean Sciences, 2nd ed. Academic Press, London, pp. 40–54.

Silvera, K., Neubig, K.M., Whitten, W.M., Williams, N.H., Winter, K., Cushman, J.C., 2010. Evolution along the crassulacean acid metabolism continuum. Funct. Plant Biol. 37, 995–1010.

Sirevåg, R., Buchanan, B.B., Berry, J.A., Troughton, J.H., 1977. Mechanisms of CO_2 fixation in bacterial photosynthesis studied by the carbon isotope fractionation technique. Arch. Microbiol. 112, 35–38.

Smith, B.N., Epstein, S., 1971. Two categories of $^{13}C/^{12}C$ ratios for higher plants. Plant Physiol. 47, 380–384.

Stanley, S.M., Yang, X., 1994. A double mass extinction at the end of the Paleozoic era. Science 266, 1340–1344.

Thomazo, C., Ader, M., Philippot, P., 2011. Extreme ^{15}N-enrichments in 2.72-Gyr-old sediments: evidence for a turning point in the nitrogen cycle. Geobiology 9, 107–120.

Tominaga, T., Minai, Y., 1984. Applications of Mössbauer spectroscopy to environmental and geochemical studies. Nucl. Sci. Appl. 1, 749–791.

Ueno, Y., Yoshioka, H., Maruyama, S., Isozaki, Y., 2004. Carbon isotopes and petrography of kerogens in ~3.5-Ga hydrothermal silica dikes in the North Pole area, Western Australia. Geochim. Cosmochim. Acta 68, 573–589.

Veizer, J., Ala, D., Azmy, K., Bruckschen, P., Buhl, D., Bruhn, F., Carden, G.A.F., Diener, A., Ebneth, S., Godderis, Y., Jasper, T., Korte, C., Pawellek, F., Podlaha, O.G., Strauss, H., 1999. 87Sr/86Sr, δ13C and δ18O evolution of Phanerozoic seawater. Chem. Geol. 161, 59–88.

Wang, Y., Jin, Y., 2000. Permian palaeogeographic evolution of the Jiangnan Basin, South China. Palaeogeogr. Palaeoclimatol. Palaeoecol. 160, 35–44.

Wignall, P.B., Sun, Y.D., Bond, D.P.G., Izon, G., Newton, R.J., Vedrine, S., Widdowson, M., Ali, J.R., Lai, X.L., Jiang, H.S., Cope, H., Bottrell, S.H., 2009. Volcanism, mass extinction, and carbon isotope fluctuations in the Middle Permian of China. Science 324, 1179–1182.

Wignall, P.B., Bond, D.P.G., Kuwahara, K., Kakuwa, Y., Newton, R.J., Poulton, S.W., 2010. An 80 million year oceanic redox history from Permian to Jurassic pelagic sediments of the Mino-Tamba terrane, SW Japan, and the origin of four mass extinctions. Glob. Planet. Chang. 71, 109–123.

Wijsman, J.W.M., Middelburg, J.J., Herman, P.M.J., Böttcher, M.E., Heip, C.H.R., 2001. Sulfur and iron speciation in surface sediments along the northwestern margin of the Black Sea. Mar. Chem. 74, 261–278.

Wilkin, R.T., Barnes, H.L., Brantley, S.L., 1996. The size distribution of framboidal pyrite in modern sediments: an indicator of redox conditions. Geochim. Cosmochim. Acta 60, 3897–3912.

Williams, L.B., Ferrell Jr., R.E., Hutcheon, I., Bakel, A.J., Walsh, M.M., Krouse, H.R., 1995. Nitrogen isotope geochemistry of organic matter and minerals during diagenesis and hydrocarbon migration. Geochim. Cosmochim. Acta 59, 765–779.

Yan, D.T., Zhang, L.Q., Qiu, Z., 2013. Carbon and sulfur isotopic fluctuations associated with the end-Guadalupian mass extinction in South China. Gondwana Res. 24, 1276–1282.

Zhang, X., Sigman, D.M., Morel, F.M.M., Kraepiel, A.M.L., 2014. Nitrogen isotope fractionation by alternative nitrogenases and past ocean anoxia. Proc. Natl. Acad. Sci. U. S. A. 111, 4782–4787.

Zhao, J.K., Sheng, J.Z., Yao, Z.Q., Liang, X.L., Chen, C.Z., Rui, L., Liao, A.T., 1981. The Changhsingian and Permian–Triassic boundary of South China. Bull. Nanjing Inst. Geol. Paleontol. Acad. Sin. 2, 1–112 (in Chinese).

Zhou, M.F., Malpas, J., Song, X.Y., Robinson, P.T., Sun, M., Kennedy, A.K., Lesher, C.M., Keays, R.R., 2002. A temporal link between the Emeishan large igneous province (SW China) and the end-Guadalupian mass extinction. Earth Planet. Sci. Lett. 196, 113–122.